International Journal of Nanomedicine

Dovepress
open access to scientific and medical research

Open Access Full Text Article

ORIGINAL RESEARCH

Photodynamic Therapy and Antibacterial Activities of a Novel Synthesized Quaternary Zn-Cu-In-S/ZnS QDs- mTHPP Porphyrin Conjugate

Ncediwe Tsolekile[1–3], Sundararajan Parani[2,3], Erenilda Ferreira de Macedo[4], Thabang Calvin Lebepe[2,3], Rodney Maluleke[2,3], Vuyelwa Ncapayi[2,3], Mangaka Clara Matoetoe[1], Sandile Phinda Songca[5], Katia Conceição[6], Dayane Batista Tada[4], Oluwatobi Samuel Oluwafemi[2,3]

[1]Department of Chemistry, Cape Peninsula University of Technology, Cape Town, 2000, South Africa; [2]Department of Chemical Sciences, University of Johannesburg, Johannesburg, 2028, South Africa; [3]Centre for Nanomaterials Science Research, University of Johannesburg, Johannesburg, South Africa; [4]Laboratory of Nanomaterials and Nanotoxicology, Institute of Science and Technology, Federal University of São Paulo, São Paulo, Brazil; [5]Department of Chemistry, University of KwaZulu-Natal, Durban, 4000, South Africa; [6]Laboratory of Peptide Biochemistry, Institute of Science and Technology, Federal University of São Paulo, São Paulo, Brazil

Correspondence: Oluwatobi Samuel Oluwafemi, Department of Chemical Sciences, University of Johannesburg, P. O. Box 17011, Doornfontein, Johannesburg, 2028, South Africa, Tel +27 011 559 9060, Email oluwafemi.oluwatobi@gmail.com; Dayane Batista Tada, Laboratório de Nanomateriais e Nanotoxicologia, Universidade Federal de São Paulo, Talim, 330 - Vila Nair, São José dos Campos, São Paulo, 12231-280, Brazil, Email day.tada@gmail.com

Background: Photodynamic therapy (PDT) is a non-invasive treatment modality that destroys abnormally growing cells or micro-organisms. Porphyrins are used as photosensitizers in PDT; however, their clinical application has been limited by their poor water solubility, resulting in aggregation and low quantum yields of reactive oxygen species (ROS).

Methods: To overcome these limitations and improve PDT efficacy, we herein report the conjugation of ZnCuInS/ZnS (ZCIS/ZnS) quantum dots (QDs) to 5,10,15,20-tetrakis(3-hydroxyphenyl)porphyrin (mTHPP). The optimal conditions for QDs porphyrin conjugation formation were systematically evaluated.

Discussion: This study further assessed the PDT efficacy and antibacterial potency of the synthesized ZCIS/ZnS-mTHPP conjugates. The PDT efficacy of the QDs, mTHPP, and conjugate was evaluated against the murine metastatic melanoma (B16 F10 Nex2) cell line. This was performed with and without LED irradiation.

Results: The conjugate exhibited the highest reduction in cell viability following LED irradiation (72%) compared to the bare QDs (19%) and mTHPP (1%). Antimicrobial studies conducted on *E. coli* showed that the conjugation exhibits a higher antibacterial effect than the bare QDs, even without light.

Conclusion: The results suggest that conjugate is a promising class of materials for anti-cancer and antimicrobial PDT.

Keywords: Zn-Cu-In-S/ZnS QDs, 5,10,15,20-tetrakis(hydroxyphenyl)porphyrin, mTHPP, photodynamic therapy, murine metastatic melanoma (B16F10-Nex2), antibacterial activity

Introduction

Cancer is a non-communicable disease classified as one of the leading silent killers worldwide. Conventional cancer treatment methods such as chemotherapy and surgery are ostracised due to their severe side effects such as tissue scarring, hair loss, accelerated hypertension etc.[1,2] Moreover, these treatment techniques are expensive, time-consuming, and limited to facilities in large hospitals.[3] This has led to the urgency to develop alternative treatment modalities, including PDT. This minimally or non-invasive treatment technique entails the generation of ROS for the destruction of abnormally growing cells or microorganisms. PDT is cost-effective and requires the injection of a photosensitizer drug (PS) followed by light administration at a particular wavelength to activate the PS for ROS generation.[4]

Amidst the number of photosensitizer drugs already tested, porphyrin compounds are the most widely used and studied in PDT due to their ability to show minimal dark toxicity, ROS generation, and ability to destroy cancer cells

Received: 15 July 2022
Accepted: 16 September 2022
Published: 15 November 2022

while sparing the healthy cells selectively.[5] Furthermore, porphyrins' structural and electronic properties can be modified by altering their peripheral substituents,[6] allowing their use in several biological applications like photothermal therapy and imaging.[7,8] While possessing such benefits, porphyrins suffer from limited solubility, aggregation in an aqueous media, and poor bio-distribution. In addition, their inability to absorb in the near-infrared (NIR) region restricts their application in treating deep-seated tumours.[9] These challenges have limited the clinical application of porphyrins in PDT. To overcome these limitations and improve the PDT efficacy of porphyrins, research has focused on the conjugation of porphyrins to biocompatible moieties such as metal–organic framework (MOF), quantum dots, nanoparticles, proteins, polymers, and ethosomes, to mention a few.[10–13]

Quantum dots are semiconductor nanomaterials with excellent tuneable optoelectronic properties (ie direct bandgap, significant Stokes shift, and long fluorescence lifetime), which permits their application in the ultra-violet to the near-infrared region.[14,15] QDs have been extensively investigated for diverse applications such as bio-labelling, imaging, and chemo-sensors.[13] Recently, ternary chalcopyrite-based QDs such as $CuInS_2$/ZnS and AgInS/ZnS QDs are emerging as a safer alternative to conventional binary chalcogenide QDs due to the absence of toxic elements (such as Cd and Pb).[15] The conjugation of porphyrins with quantum dots (QDs) has gained momentum due to the uniquely tuneable optical and electronic properties of QDs. Previously, our group reported the improvement of singlet oxygen generation of porphyrins and the progress of their cell internalization by conjugation with QDs.[16] Compared to binary and ternary QDs, quaternary QDs (eg ZCIS/ZnS) possess unique optical properties with high resistance to photo-quenching, tuneable bandgap, enhanced photo-luminescence quantum yields (PLQYs), and narrow emissions spectra.[18,19] Noting these results and the upsurge in studies focusing on nanoparticle-porphyrin conjugates,[9,11,20,21] as far as we know, there has been no report on quaternary QD-porphyrin conjugates for PDT and antimicrobial applications.

Herein, we report the synthesis, luminescence, and structural properties of ZCIS/ZnS QDs; mTHPP and the successful conjugation of ZCIS/ZnS QDs to mTHPP. The as-synthesized materials were characterized using various optical and morphology techniques such as photoluminescence (PL), Ultraviolet-visible spectrophotometry (UV–Vis), X-ray diffraction (XRD), Transmission electron microscopy (TEM) and Fourier Transform Infrared spectroscopy (FT-IR). Following successful synthesis, photodynamic therapy efficacy using the QDs, mTHPP and conjugate was evaluated against the murine metastatic melanoma cell line (B16F10-Nex2) both in the presence and absence of light. Furthermore, the antimicrobial photodynamic therapy (aPDT) efficiency of the as-synthesized materials was evaluated against *E. coli* (ATCC 25922). The results showed the as-synthesized ZCIS/ZnS-mTHPP conjugate to be a valuable material and efficient PS for PDT and aPDT applications. Moreover, the conjugate addressed the shortcomings of porphyrins such as water insolubility, lack of NIR absorption, improvement in the cytotoxicity and photodynamic therapy efficacy of the porphyrins.

Materials and Methods

Chemicals

Copper chloride ($CuCl_2$), indium chloride ($InCl_3$), sodium citrate dihydrate ($Na_3C_6H_5O_7$), L-glutathione (GSH), sodium sulphide (Na_2S), zinc acetate dihydrate ($Zn(O_2CCH_3)_2(H_2O)_2$), thiourea (CH_4N_2S), sodium hydroxide (NaOH), hydrochloric acid (HCl), ethanol (CH_3CH_2OH), dichloromethane (CH_2Cl_2), methanol (CH_3OH), pyrrole (C_4H_4NH), n-hexane (C_6H_{14}), 3-hydroxybenzaldehyde ($C_7H_6O_2$), propionic acid ($CH_3CH_2CO_2H$), chloroform ($CHCl_3$), sodium bicarbonate ($NaHCO_3$), acetone ($(CH_3)_2CO$), and ethyl acetate ($CH_3COOCH_2CH_3$), were purchased from Sigma Aldrich, South Africa and used as received. RPMI medium, fetal bovine serum, and Mueller Hinton (MH) agar plates. Deionized water was used for the synthesis and analysis.

Synthesis of ZCIS QDs and ZCIS/ZnS QDs

Synthesis of ZCIS QDs

The ZCIS QDs were synthesized based on our previously reported method on ternary CIS/ZnS QDs with slight modifications.[16] Briefly, $CuCl_2$ (0.011 g, 0.063 mmol) and $InCl_3$ (0.055 g, 0.25 mmol) were added to 100 mL of deionized water under magnetic stirring. This was followed by the addition of $Zn(O_2CCH_3)_2(H_2O)_2$ (20.4 mg, 0.093 mmol), $Na_3C_6H_5O_7$ (0.294 g, 1.00 mmol) and GSH (0.09 g, 0.29 mmol). The pH of the solution was adjusted to 3.60 (using 0.1 M NaOH/0.1 M HCl), followed by the addition of Na_2S solution (1.95g/25mL, 25.00 mmol) under magnetic

stirring to initiate the reaction. The solution was then heated for 45 mins at 95°C to produce ZCIS QDs. The amount of Zn was further varied to 0.031; 0.063, and 0.093 mmol to investigate the effect of Zn on the optical properties of the ZCIS core QDs.

Synthesis of ZCIS/ZnS QDs

ZCIS/ZnS core/shell QDs were prepared by adding a solution of $Zn(O_2CCH_3)_2(H_2O)_2$ (0.044 g, 0.200 mmol) and CH_4N_2S (0.015 g, 0.200 mmol) to the ZCIS QDs solution under reflux for 45 min. The solution was heated at 95°C for 1 h 20 min to produce ZCIS/ZnS QDs. The addition of ethanol precipitated the QDs. The resulting supernatant was discarded, and the precipitate was centrifuged, washed with ethanol, and dried.

Synthesis of mTHHP

The synthesis of mTHPP was carried out according to Tsolekile et al.[16] In a typical reaction, 3-hydroxybenzaldehyde (2.50 g, 20.47 mmol) was added to propionic acid (15 mL) in a 100 mL round-bottom flask equipped with a magnetic stirring bar and refluxed for 15 min at 140°C. Distilled pyrrole (1.42 mL, 20.469 mmol) was added quickly to the mixture and refluxed for an additional 1.5 h. After the reflux, excess propionic acid was evaporated at 220°C. The material was cooled to room temperature and neutralized with the aqueous solution of $NaHCO_3$ (5%). The precipitated crude porphyrin was washed with chloroform and finally chromatographed on a silica gel column using an ethyl acetate: n-hexane (2:1, v/v) mixture as eluent. ^{1}H NMR ($CDCl_2$) δ, ppm: −2.89 (s,2H, NH), 7.21(d, 8H, ArH, J=0.016 Hz), 8.00(d,8H,ArH, J=0.017 Hz), 8.86(s,7H, B-H), 9.97 (s,3H, O-H). UV-vis λ_{max} (MeOH): Soret (418 nm) and Q-bands (516, 555, 595, 650 nm).

Conjugation of ZCIS/ZnS QDs to mTHPP

An aqueous solution of the synthesized ZCIS/ZnS QDs (20 mg/20 mL H_2O) was prepared and added to mTHPP (1 mg/ 10 mL CH_3OH), followed by stirring for 1 hr. A ratio of 3:1, v/v (QDs: mTHPP), was maintained when preparing the conjugate.

Characterization

The as-synthesized QDs, mTHPP and conjugate were characterized using; Ultraviolet-visible spectroscopy (UV-vis) (Perkin Elmer UV-vis Lambda 25 spectrometer, UK); Photoluminescence (PL) spectroscopy (RF-6000, Shimadzu, Japan), Fourier Transform Infrared spectroscopy (FT-IR) (Spectrum two UATR spectrometer, Perkin Elmer, UK), Transmission electron microscopy (TEM) (JEOL-2100) and X-ray diffraction (XRD) (PANalytical X'Pert. Xray diffractometer using a monochromatic Cu Kα radiation (λ = 0.15406 nm) at room temperature). Nuclear Magnetic Radiation (^{1}H NMR, 500 MHz Bruker spectrometer).

Biological Studies

Cytotoxicity and Photocytoxicity

Cell viability assays were performed to evaluate the photocytoxicity (cytotoxicity under irradiation) and cytotoxicity in the dark (cytotoxicity in the absence of irradiation) against the cancer cell models (B16F10-Nex2 cell line). The murine melanoma cell line B16F10 was initially obtained from the Ludwig Institute for Cancer Research, São Paulo (Brazil). The B16F10-Nex2 clone used in our study was established at the "Unidade de Oncologia Experimental", Escola Paulista de Medicina, Universidade Federal de São Paulo (UNIFESP), Brazil. The fully characterized B16F10-Nex2 melanoma cell line was deposited in the "Banco de Células do Rio de Janeiro" (BCRJ, Brazil), no. 0342. The cells were plated at 1×10^4 cells/well. Two plates were prepared precisely in the same way. One was irradiated, while the other was wrapped in aluminium paper outside the incubator for the time used to irradiate the first plate. The two plates were incubated for 24 h before adding the samples. To add the samples, the medium was withdrawn from all the wells, and 200 µL of fresh RPMI medium containing 10% fetal bovine serum was added. To each well, 50 µL of the sample was added. The two plates were incubated for 24 h.

Irradiation: The 200 µL of medium with the 50 µL of the sample was withdrawn from each well and replaced with 100 µL of phosphate buffer saline (PBS). One of the plates was irradiated at 660 nm for 300 seconds (51 J/cm^2). During this time, the

other plate was wrapped in aluminium paper outside the incubator inside the laminar flux. The 100 µL of PBS was replaced by a culture medium (RPMI+10% fetal bovine serum). Both plates were incubated for 24 h.

Cell viability was then evaluated by the MTT method. PBS replaced the culture medium to wash out reminiscent samples and avoid cell death by dryness due to the time it takes to finish the withdrawal of the RPMI from all the wells. Thereafter PBS was replaced by a 0.5 mg/mL 3-(4,5-dimethylthiazol-2yl)-2,5-diphenyltetrazolium bromide (MTT) solution. Both plates were incubated for 3 h. The MTT solution was carefully withdrawn from all the wells and replaced by dimethyl sulfoxide (DMSO) to dissolve the formazan salt. The absorbance of each well was measured at 540 nm in a plate reader (Biotek). Cell viability was calculated by considering the average absorbance of the wells incubated without samples and irradiation as 100% of cell viability. The values are presented as mean values and standard deviation (n=7).

Antibacterial Activity Against *E. coli*

Antibacterial activity of the conjugate, mTHPP and QDs were evaluated against *E. coli* (ATCC 25922) by the potting-and-tilt-spreading (SATS) method as described in Thomas et al,[21] and Oliveira et al.[22] The bacteria were activated in Mueller Hinton (MH) agar plate and incubated for 24 h at 37 ◦C. Following this, a suspension of bacteria was prepared in NaCl solution (0.9%). The optical density (OD) was set to 0.3 at 600 nm, corresponding to 10^8 cells/mL using a plate reader (Synergy H1-Biotek). The suspension was diluted to 10^6 cells/mL, using the stock solution of MH broth as a culture medium. Two 96-well plates were prepared using this diluted cell suspension (10^6 cells/mL) to incubate the samples with the bacteria. Different concentrations of each sample (Stock solutions; QD: 1.1 mg/mL; mTHPP: 0.375 mg/mL; Conjugate (0.25 mg/mL + mTHPP): (0.08 mg/mL); DMSO and ultrapure water (ddH_2O) were used as negative controls) were evaluated. The plates were incubated for 3 h at 37 ˚C. After this time, one of the plates was irradiated at 660 nm (LED; 164.51 J/cm^2). Then, the plate was incubated at 37 ˚C, completing 20 h of incubation. The second plate was not irradiated but incubated at 37 ˚C for 20 h. For SATS, the inoculum and sample/suspension from each well were applied as micro drops (10 µL) and spread on the MH agar surface by tilting or gently swirling the plate. After surface drying (5–6 min), the plates were sealed singly in clear plastic covers to avoid external contaminants and dehydration and were incubated upside down at 37°C. The presence of colonies of bacteria was identified after 24 h.

Results and Discussion

The quantum dots were synthesized using an eco-friendly reflux method in an aqueous medium. The amount of Zn^{2+} used during synthesis was varied while keeping the Cu:In ratio at 1:4 and other experimental properties constant. Figure 1 shows the UV absorption and photoluminescence spectra of the QDs prepared at different Zn amounts. The absorption spectra of QDs showed broad bands in the UV-vis region, characteristic of chalcopyrite QDs. The absorption onset of the QDs gradually shifted blue when the amount of Zn was increased from 0.093 mmol to 0.031 mmol suggesting a bandgap tuning (Figure 1A inset). The corresponding photoluminescent spectra of the resulting QDs are shown in Figure 1B. The QDs exhibited broad PL

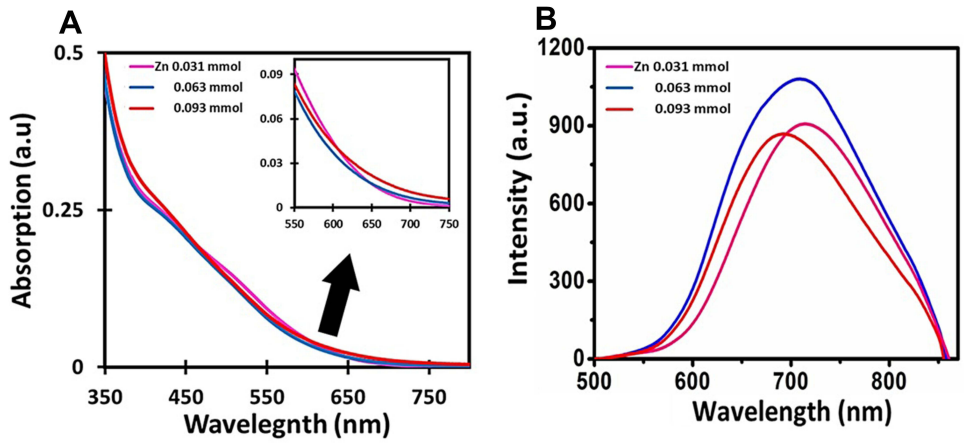

Figure 1 (**A**) UV–vis absorption (measured in distilled water) and (**B**) PL spectra of ZCIS QDs at different amounts of Zn.

emission peaks with full width half maximum ranges (FWHM) from 164–172 nm. This is in line with previous studies on quaternary QDs.[23–27] The PL peak position of the QDs is blue-shifted (from 713 to 694 nm) as the amount of Zn increased from 0.031 mmol to 0.093 mmol about the absorption spectra. Based on the high PL intensity, 0.063 mmol was selected as the optimum amount of Zn used to synthesize the QDs.

The synthesized QDs were modified by passivating with a ZnS shell. During the passivation process, Zn^{2+} was varied while keeping the Zn:S ratio of (1:1) constant. The UV-vis absorption spectra of core/shell QDs (Figure 2A) show broad absorption spectra similar to core QDs. However, at 0.40 mmol of Zn, the absorption tail extended to the NIR region, suggesting that a high Zn concentration produces more defects.[17] The PL maximum of the core/shell QDs becomes red-shifted from 691 nm to 718 nm (Figure 2B) as the Zn ion increases from 0.1 to 0.4 mmol. The maximum intensity was obtained at 0.10 mmol Zn concentration with an emission maximum peak at 706 nm. The increase in the PL intensity can be attributed to the surface defects elimination by passivation with the ZnS shell.[17] The significant decrease in the PL intensity at high Zn concentration (0.4 mmol) also supports the presence of more defects, as seen in the corresponding UV-vis absorption spectra. In general, ternary QDs such as CIS QDs exhibit blue-shifted emission in the PL spectra after passivation with ZnS QDs due to partial alloy formation by ion exchange at the core/shell interface. However, such blue-shifted emission after passivation was not observed in these quaternary QDs, indicating the successful quaternary core/shell structure formation.

The shape and particle size of the as-synthesized core QDs and core/shell QDs were determined using the TEM. The as-synthesized QDs were mono-dispersed and nearly spherical. The approximate diameters of the core QDs and core/shell QDs are 2.5 nm and 3.1 nm, respectively (Figures 3A and Figure 3). The increase in size after the shell growth could be attributed to the ZnS shell's passivation of the core QDs.

Powdered XRD analysis of the as-synthesized QDs in Figure 3C consists of three broad peaks for core QDs and core/shell QDs. The obtained 2θ values of ZCIS QDs at 28.1◦, 46.4◦, and 55.2◦ corresponding to diffraction patterns (112), (204) and (302) indexed to lie between chalcopyrite and the wurtzite crystal phases of CIS QDs. The ZCIS/ZnS QDs exhibited similar diffraction peaks; however, at higher angles (29.4◦, 48.9◦ and 56.9◦) with increased intensity was observed after ZnS passivation, confirming the successful formation of the ZCIS/ZnS QDs core/shell structure. These results are consistent with the literature reports.[28] Debye Scherrer equation was used to calculate the average particle size using the XRD, where:

$$D = \frac{K.\lambda}{(\beta \cos\theta)}$$

D is the mean size of crystallites (nm), K is crystallite shape factor, a good approximation is 0.9, λ is the X-ray, B is the full width at half the maximum (FWHM) in radians of the X-ray diffraction peak, and θ is the Braggs' angle (deg.). The average particle size according to the XRD was 1.94 nm for ZCIS/ZnS QDs, which increased to 2.10 nm after the formation of the (Z)CIS/ZnS QDs.

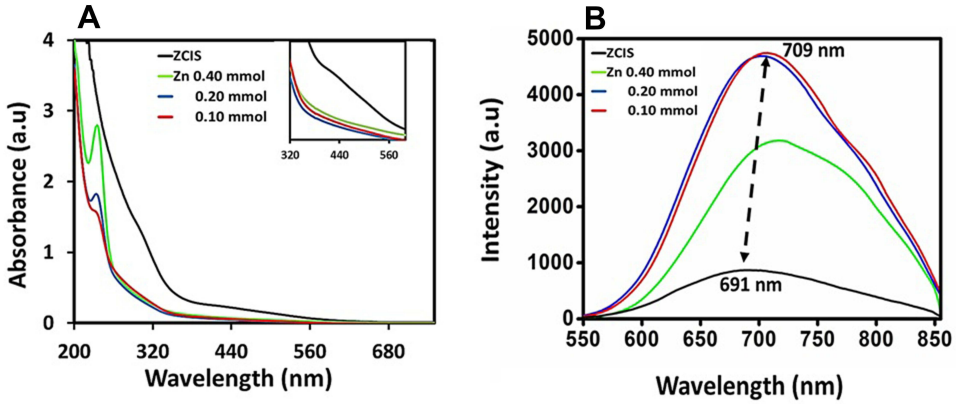

Figure 2 (**A**) UV (measured in distilled water) and (**B**) PL spectra of ZCIS/ZnS core/shell QDs are different concentrations of Zn^{2+}.

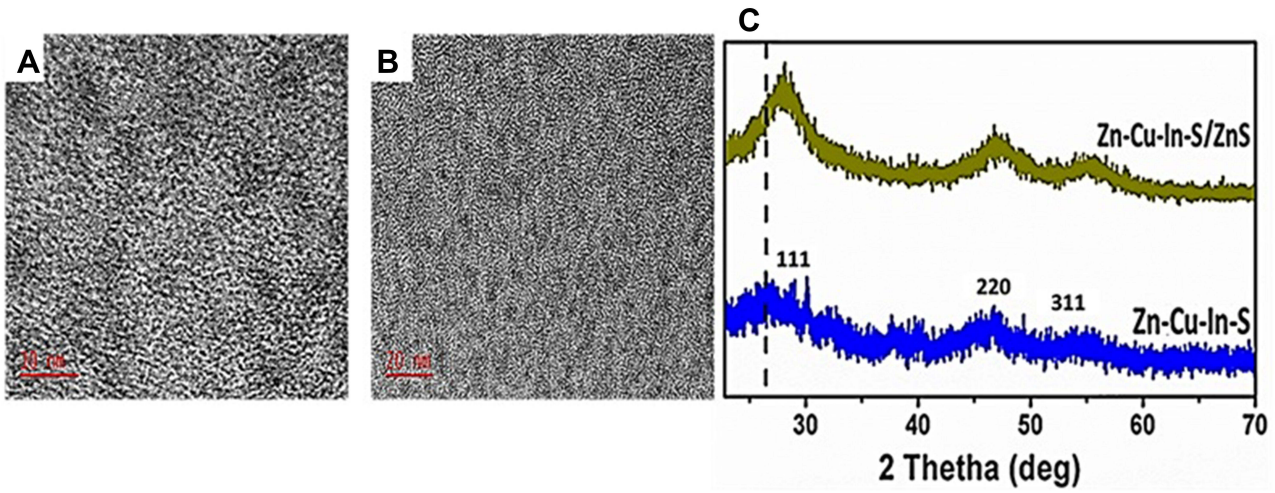

Figure 3 TEM micrographs of (**A**) ZCIS QDs and (**B**) ZCIS/ZnS QDs. (**C**) XRD overlay of ZCIS QDs and ZCIS/ZnS QDs.

Spectroscopic Characterization of mTHPP and ZCIS/ZnS-mTHPP Conjugate

Following the synthesis of mTHPP via the condensation of benzaldehyde with pyrrole in an acidic medium, the porphyrin were purified via silica gel column chromatography. The molar extinction coefficient value was 2.56 $M^{-1}cm^{-1}$ as measured in methanol. mTHPP exhibited characteristic patterns in the ^1H NMR ($CDCl_2$) spectra; the peak at −2.89 confirms the successful synthesis of free-base porphyrin (Figure S1). The absorption spectra (Figure 4A) of the bare mTHPP exhibited an intense Soret band at 418 nm, attributed to the strong transition of $S_0 \rightarrow S_2$ and four Q-bands (516, 555, 595, 650 nm) attributed to the weak $S_0 \rightarrow S_1$ transition.[11]

ZCIS/ZnS-mTHPP conjugate: The ZCIS/ZnS QDs were mixed with mTHPP to prepare the ZCIS/ZnS-mTHPP conjugate. The amount of the QDs was varied to optimize the conjugation. Conjugation of mTHPP – QDs is predicted to have been achieved via direct esterification. This is expected to have occurred via the electronic coupling (conjugation) between the carboxyl groups of glutathione-capped QDs surface and the electron-rich methoxy-substituted phenyl rings of the porphyrin. With increasing the ZCIS/ZnS QDs in the conjugate, the Soret band gradually broadened and split into two peaks (Figure 4B). The splitting of the Soret and Q-band maxima of the porphyrin after the addition of nanomaterials has been reported and attributed to several phenomena such as (i) the orientation of the porphyrin on the QDs, (ii) strong exciton-coupling, (iii) significant distortion of the D4h symmetry induced by the presence of a substituent (iv), strong intramolecular and intermolecular π–π interactions of porphyrin macrocycles, and (v) the intense mixing of the Soret, Q states and relatively high intensity of the Q-bands.[28–33] The four Q-bands of mTHPP are seen as small humps (Figure 4C) with a slight redshift in the conjugate, indicating

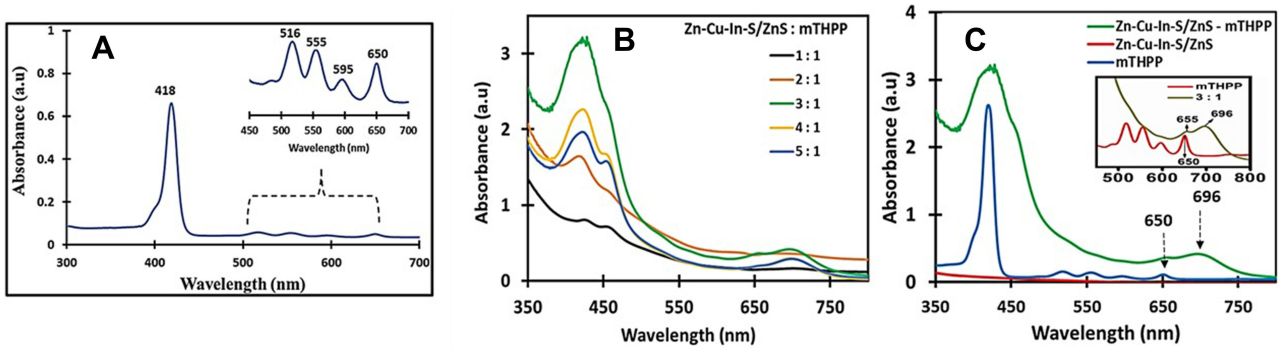

Figure 4 (**A**) Absorption spectra of mTHPP (measured in methanol), (**B**) ZCIS/ZnS–mTHPP conjugates (measured in methanol:H_20-) (**C**) magnified Q band spectra of ZCIS/ZnS-mTHPP conjugates at 3:1 v/v ratio in comparison to that of mTHPP.

successful interaction of mTHPP with QDs. In contrast, the development of the new peak in the NIR region at 696 nm with high intensity at 3:1 v/v (ZCIS/ZnS: mTHPP) ratio suggests an extension in the π-conjugated ZCIS/ZnS-mTHPP system. Based on these results, the ratio 3:1 v/v (ZCIS/ZnS: mTHPP) was selected as the optimum ratio for the conjugate preparation.

FTIR spectroscopy was used to characterize and confirm the conjugate (ZCIS/ZnS- mTHPP) formation (Figure 5). mTHPP porphyrin exhibited characteristic bands at 3321 cm^{-1}, 2921 cm^{-1}, and 1599 $cm^{-1,}$ which were attributed to the presence of νNH pyrrole, νCH, and νC=C vibrations, respectively, within its structure. For ZCIS/ZnS QDs, asymmetric and symmetric νCOO, νOH and νCH vibrations from the surface capping GSH groups were observed at 1568 cm^{-1}, 1384 cm^{-1}, 3284 cm^{-1}, and 2959 $cm^{-1,}$ respectively. The spectra of the conjugate resemble the QDs spectra; however, the asymmetric and symmetric νCOO bands are shifted to higher wavenumbers (1604 cm^{-1} and 1392 $cm^{-1,}$ respectively) compared to bare QDs, which suggests the linkage of QDs with mTHPP via esterification as shown in the schematic representation (Scheme 1).

PDT Analysis

Unconjugated porphyrins have displayed synergetic effects on cancer cells, while porphyrin conjugation has proved to improve on these properties and enable dual functionality of the conjugates. In photodynamic therapy, the conjugation of porphyrins to QDs is highly beneficial as the conjugate acquires the structural functionalities and singlet oxygen generation abilities from the porphyrins while also gaining the bio-distribution, luminescence, and specificity of QDs.[34] Herein, the PDT efficacy of the as-synthesized ZCIS/ZnS-mTHPP conjugate was evaluated against the B16F10-Nex2 cell line. Cell viability measurements evaluated the PDT efficacy after treatment of the cells with the conjugate at various concentrations. For comparative purposes, cell viability was also measured after incubating the cells

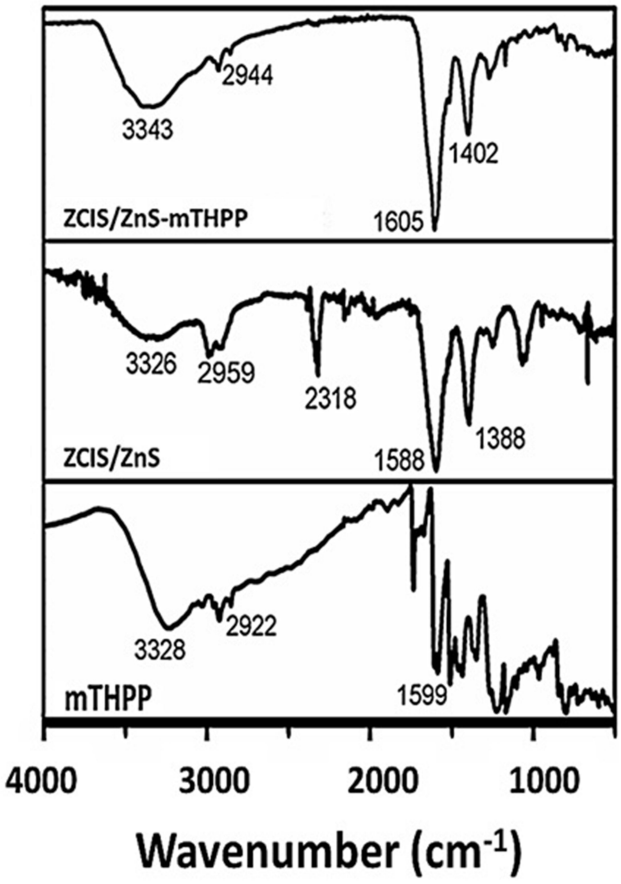

Figure 5 FTIR spectra of ZCIS/ZnS QDs, mTHPP and ZCIS/ZnS-mTHPP.

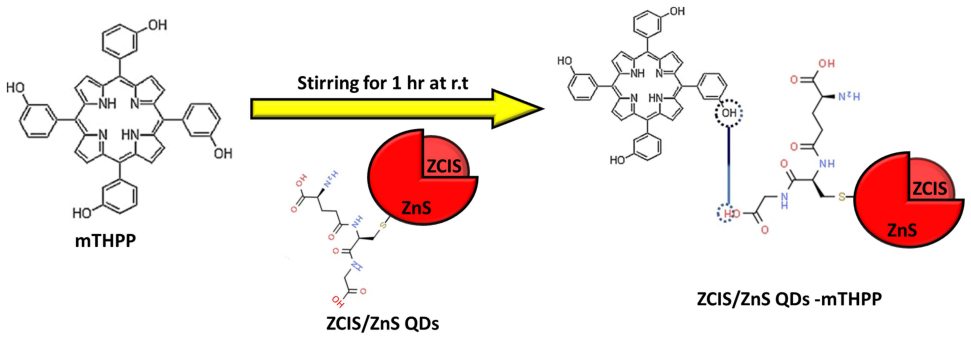

Scheme 1 Schematic representation of chemical linkage between ZCIS/ZnS QDs and mTHPP.

with the QDs and mTHPP, with and without laser irradiation. Incubation of the cells with the QDs at 0.220 mg/mL and 0.110 mg/mL showed good values of viabilities, 71±6% and 92±5%, respectively, pointing out their very low cytotoxicity in the dark (cell viability without laser irradiation) (Figure 6). After laser irradiation, the viability of the cells reduced to 52± 4% and 74±7% after exposure to 0.220 mg/mL and 0.110 mg/mL of the QDs, respectively. When mTHPP was used in the solution, it exhibited dose-dependent cytotoxicity against the cells without light and under irradiation. At 0.015 mg/mL and 0.008 mg/mL, cell viabilities in the dark were 51% and 100% respectively. After laser irradiation, cell viabilities were reduced to 47±2% at 0.015 mg/mL and 45±2% at 0.008 mg/mL.

The conjugate exhibited a remarkable reduction in the viability of the cells under irradiation. In contrast, cytotoxicity in the dark was close to that of the QDs and higher than that of mTHPP in the solution. The conjugate composed of 0.016 mg/mL of mTHPP and 0.05 mg/mL core/shell QDs showed cell viability of 70±7% in the absence of light irradiation which was reduced mainly to 7± 0% upon laser irradiation. When the amounts of the conjugate were decreased to 0.008 mg/mL and 0.025 mg/mL, respectively, the conjugate promoted cell viability of 84±5% in the dark, which was reduced to 12±1% under irradiation. In comparison, the conjugate induced a more prominent decrease in cell viability

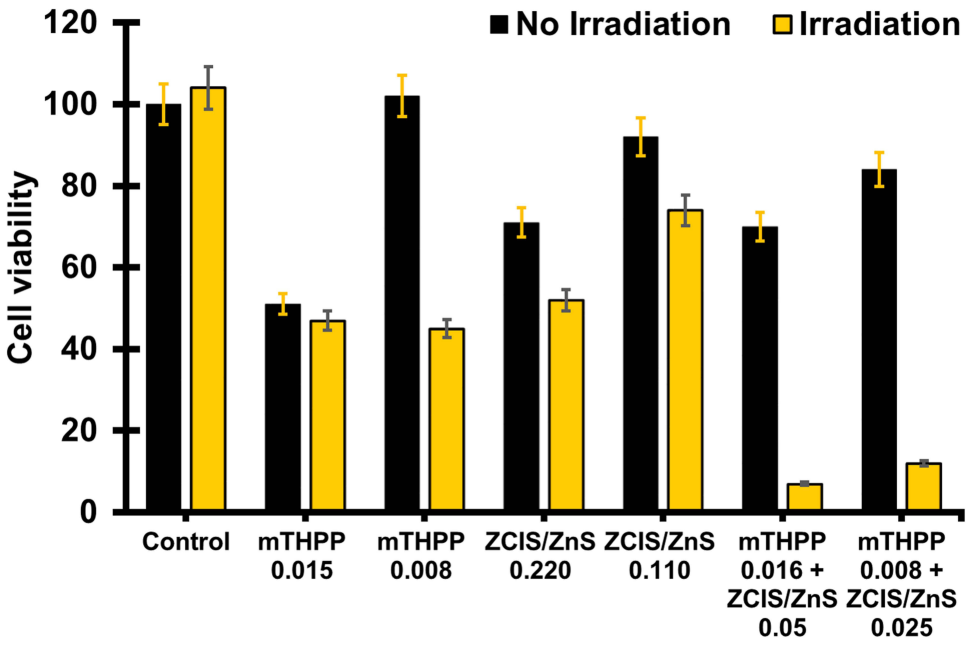

Figure 6 Cell viabilities study against B16 F10 Nex2 cells at different concentrations of ZCIS/ZnS QDs, mTHPP and ZCIS/ZnS-mTHPP conjugate with and without irradiation (Irradiation wavelength = 660 nm for 300 seconds (51 J/cm^2)).

(72%) than the core/shell QDs (19%) and mTHPP (1%) when irradiated. These results indicate that the conjugate could serve as a promising photosensitizing system for enhanced PDT efficiency.

Antibacterial Activity Against *E. coli*

The high incidence of antibiotic resistance has led medical research to study alternative methods to fight bacteria and related microorganisms. The antibacterial activity effect of varying concentrations of the core/shell QDs, mTHPP and the conjugate against *E. coli* was evaluated via the SATS method. Figure 7 shows the digital images of petri dishes of the SATS method showing bacteria colonies after incubation with the core/shell QDs, mTHPP and the conjugate. The core/shell QDs (0.220 mg/mL) and mTHPP (0.015 mg/mL) were found to be bactericidal only in the presence of laser irradiation. The conjugate proved to be bactericidal in the presence and absence of laser irradiation. This indicates increased interaction of the conjugate with *E. coli*, thereby displaying improved antibacterial efficiency compared to the bare core/shell QDs and mTHPP. Control groups are shown in Figures 7D and Figure 7E. In addition, the result obtained with a positive control group is shown in Figure S2. It was possible to note that the results observed with quantum dots and mTHPP under irradiation as well as with the conjugate in the absence and presence of irradiation were equivalent to the results observed by using antibiotics. Few studies have been reported on the bactericidal activity of conjugated QDs. Studies of ZnO QDs by Preeti et al[35] exhibited dose-dependent, broad-spectrum

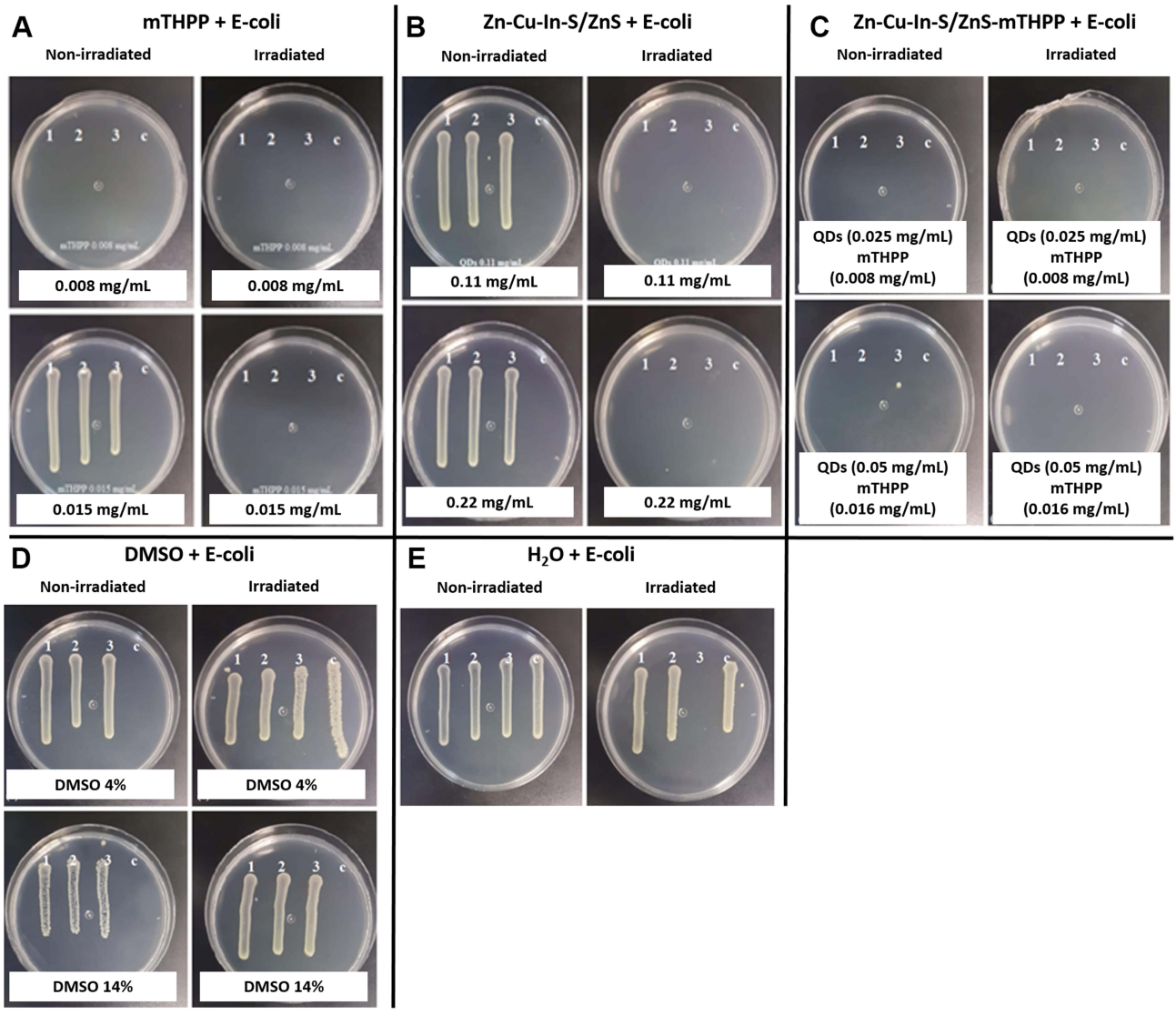

Figure 7 Seeding of the *E. coli* incubated with (**A**) mTHPP, (**B**) Zn-Cu-In-S/ZnS, (**C**) Zn-Cu-In-S/ZnS-mTHPP, (**D**) DMSO and (**E**) water.

microbicidal activity against all MDR isolates of *E. coli* and *C. albicans*. Our results showed that the conjugate could serve as a potential photosensitizing drug in PDT, antibacterial and aPDT applications.

Conclusion

In conclusion, ZCIS/ZnS core/shell QDs were synthesized via a one-pot eco-friendly reflux method. The as-synthesized core/shell QDs were conjugated to mTHPP to fabricate a water-soluble and biocompatible ZCIS/ZnS-mTHPP conjugate which showed improved optical properties and superior biological activities compared to the bare core/shell QDs and the porphyrin. Photodynamic therapy efficacy of the core/shell QDs, mTHPP, and the conjugate was evaluated by exposing the murine metastatic melanoma B16F10-Nex2 cell line to various concentrations of the as-synthesized materials with and without laser irradiation. The cell viability results revealed that the conjugate is as biocompatible with B16F10-Nex2 cells as the mTHPP alone in the absence of light. In the presence of light, the conjugate showed excellent PDT activity towards B16F10-Nex2 cells allowing cell viability of only 7%, which is far more effective than the result obtained with mTHPP (47% allowing cell viability of 43) and the core/shell QDs (75%) even at lower core/shell QD concentration in the conjugate. We suggest that the core/shell QDs and mTHPP can be considered bactericidal against *E. coli*, a Gram-negative strain, in the presence of laser irradiation; in contrast, the conjugate was effective with and without laser irradiation. These results showed the as-synthesized conjugate as a promising photosensitizing drug with high potency for application in photodynamic therapy of cancer and as an antibacterial agent.

Acknowledgments

The authors would like to acknowledge National Research Foundation (NRF), South Africa, under the Nanotechnology Flagship Programme (Grant no: 97983), Competitive Programme for Rated Researchers (Grant no: 106060 and 129290), Thuthuka (Grant No: 121986), equipment-related travel and training (Grant no 109892), Cape Peninsula University of Technology, the University of Johannesburg research committee (URC) and Faculty of Science research committee (FRC) for funding. We also thank Fundação de Amparo à Pesquisa do Estado de São Paulo (FAPESP: 2019/20111-8) for funding Oluwatobi Samuel Oluwafemi for the trip to Sao Paulo.

Disclosure

The authors declare no conflicts of interest in this work.

References

1. Wait S, Hana D, Muthu V, et al. Towards sustainable cancer care: reducing inefficiencies, improving outcomes—A policy report from the all can initiative. *J Cancer Policy*. 2017;13:47–64. doi:10.1016/j.jcpo.2017.05.004
2. Cui F, Zhou Z, Zho HS. Review—measurement and analysis of cancer biomarkers based on electrochemical biosensors. *J Electrochem Soc*. 2020;16:037525. doi:10.1149/2.0252003JES
3. Yanovsky RL, Bartenstein DW, Rogers S, Isakoff SJ, Chen ST. Photodynamic therapy for solid tumors: a review of the literature. *Photodermatol Photoimmunol Photomed*. 2019;35:295–303. doi:10.1111/phpp.12489
4. Abdulaeva IA, Birin KP, Bessmertnykh-Lemeune A, Tsivadze AY, Gorbunova YG. Heterocycle-appended porphyrins: synthesis and challenges. *Coord Chem Rev*. 2020;407:213108. doi:10.1016/j.ccr.2019.213108
5. Wei W, Li W, Xiaa B, Zhang H, Bai F. Theoretical investigations of the aromaticity, stability and photophysical behaviors for expanded porphyrins. *Chem Phys Lett*. 2019;728:25–31. doi:10.1016/j.cplett.2019.04.067
6. Su S, Ding Y, Li Y, Wu Y, Nie G. Integration of photothermal therapy and synergistic chemotherapy by a self-assembled porphyrin micelle confer chemosensitivity in triple-negative breast cancer. *Biomaterials*. 2016;80:169–178. doi:10.1016/j.biomaterials.2015.11.058
7. Carneiro J, Goncalves A, Zhou Z, Griffin KE, Kaufman NEM, Vicente MGH. Synthesis and in vitro PDT evaluation of new porphyrins containing meso-epoxymethylaryl cationic groups. *Lasers in Surg Med*. 2018;50:566–575. doi:10.1002/lsm.22824
8. Hurtado CR, Hurtado GR, de Cena GL, et al. Diamond nanoparticles-porphyrin mTHPP conjugate as photosensitizing platform: cytotoxicity and antibacterial activity. *Nanomaterials*. 2021;11:1393. doi:10.3390/nano11061393
9. Makola LC, Manage M, Nyokong T. Enhancement of photodynamic antimicrobial therapy through the use of cationic indium porphyrin conjugated to Ag/$CuFe_2O_4$ nanoparticles. *Photodiagnosis Photodyn Ther*. 2020;30:101736. doi:10.1016/j.pdpdt.2020.101736
10. Qin JH, Zhang H, Sun P, et al. Ionic liquid induced highly dense assembly of porphyrin in MOF nanosheets for photodynamic therapy. *Dalton Trans*. 2020;49:17772–17778. doi:10.1039/D0DT03031G
11. Yang M, Cao S, Sun X, et al. Self-assembled naphthalimide conjugated porphyrin nanomaterials with D-A structure for PDT/PTT synergistic therapy. *Bioconjug Chem*. 2020;31:663–672. doi:10.1021/acs.bioconjchem.9b00819
12. Lv G, Guo W, Zhang W, et al. Near-infrared emission CuInS/ZnS quantum dots: all-in-one theranostic nanomedicines with intrinsic fluorescence/photoacoustic imaging for tumor phototherapy. *ACS Nano*. 2016;10:9637–9645. doi:10.1021/acsnano.6b05419

13. Li H, Jiang X, Wang A, Chu X, Du Z. Simple synthesis of $CuInS_2$/ZnS core/shell quantum dots for white light-emitting diodes. *Front Chem*. 2020;8:1–9. doi:10.3389/fchem.2020.00001
14. Frick JJ, Cheng G, Kushwaha S, et al. Observation of [VCu1−Ini2+VCu1−] defect triplets in Cu-Deficient $CuInS_2$. *J Phys Chem C*. 2020;124:26415–26427. doi:10.1021/acs.jpcc.0c08872
15. Nguyen AT, Gao F, Baucom D, Heyes CD. $CuInS_2$-Doped ZnS quantum dots obtained via non-injection cation exchange show reduced but heterogeneous blinking and provide insights into their structure−optical property relationships. *J Phys Chem C*. 2020;124:10744–10754. doi:10.1021/acs.jpcc.0c01933
16. Tsolekile N, Nahle S, Zikalala N, et al. Cytotoxicity, fluorescence tagging and gene-expression study of CuInS/ZnS QDS - meso(hydroxyphenyl) porphyrin conjugate against human monocytic leukemia cells. *Sci Rep*. 2020;10:4936. doi:10.1038/s41598-020-61881-8
17. Jia Y, Wang H, Xiang L, et al. Tunable emission properties of core-shell ZnCuInS-ZnS quantum dots with enhanced fluorescence intensity. *J Mater Sci Technol*. 2018;34:942–948. doi:10.1016/j.jmst.2017.07.014
18. Guo W, Chen N, Tu Y, et al. Synthesis of Zn-Cu-In-S/ZnS core/shell quantum dots with inhibited blue-shift photoluminescence and applications for tumor targeted bioimaging. *Theranostics*. 2013;3:99–108. doi:10.7150/thno.5361
19. Samperi M, Limón D, Amabilino DB, Pérez-García L. Enhancing singlet oxygen generation by self-assembly of a porphyrin entrapped in supramolecular fibers. *Cell Reports Phys Sci*. 2020;1:100030. doi:10.1016/j.xcrp.2020.100030
20. Kirar S, Thakur NS, Laha JK, Banerjee UC. Porphyrin functionalized gelatin nanoparticle-based biodegradable phototheranostics: potential tools for antimicrobial photodynamic therapy. *ACS Appl Bio Mater*. 2019;2:4202–4212. doi:10.1021/acsabm.9b00493
21. Thomas P, Mujawar MM, Sekhar AC, Upreti R. Physical impaction injury effects on bacterial cells during spread plating influenced by cell characteristics of the organisms. *J Appl Microbiol*. 2014;116:911–922. doi:10.1111/jam.12412
22. Oliveira RL, Barbosa L, Hurtado CR, et al. Bioglass-based scaffolds coated with silver nanoparticles: synthesis, processing and antimicrobial activity. *J Biomed Mater Res Part A*. 2020;108:2447–2459. doi:10.1002/jbm.a.36996
23. Deng D, Qu L, Cheng Z, Achilefu S, Gu Y. Highly luminescent water-soluble quaternary Zn–Ag–In–S quantum dots and their unique precursor S/In ratio-dependent spectral shifts. *J Lumin*. 2014;14:364–367. doi:10.1016/j.jlumin.2013.09.063
24. Nadya JE, Ali M, Kamel OA, Ebrahim S, Soliman M. Room temperature synthesis of aqueous ZnCuInS/ZnS quantum dots. *J Dispers Sci Technol*. 2020;13:1956–1962. doi:10.1080/01932691.2019.1645022
25. Jawhar NN, Soheyli E, Yazici AF, Mutlugun E, Sahraei R. Preparation of highly emissive and reproducible Cu-In-S/ZnS core/shell quantum dots with a mid-gap emission character. *J Alloys Compd*. 2020;824:153906. doi:10.1016/j.jallcom.2020.153906
26. Liu C, Tong X, Channa AI, et al. Tuning the composition of heavy metal-free quaternary quantum dots for improved photoelectrochemical performance. *J Mater Chem A*. 2021;9:5825–5832. doi:10.1039/D0TA11481B
27. Chen T, Xu Y, Xie Z, Wang L, Jiang JW, Jiang W. One-pot synthesis of water-soluble Cu–In–Zn–S/ZnS core/shell quantum dots for efficient white light-emitting devices. *Opt Mater*. 2020;105:109885. doi:10.1016/j.optmat.2020.109885
28. Pan D, Liang P, Zhong X, et al. Self-assembled porphyrin-based nanoparticles with enhanced near-infrared absorbance for fluorescence imaging and cancer photodynamic therapy. *ACS Appl Bio Mater*. 2019;2:999–1005. doi:10.1021/acsabm.8b00530
29. Arooj Q, Wilson GJ, Wang F. Shifting UV-vis absorption spectrum through rational structural modifications of zinc porphyrin photoactive compounds. *RSC Adv*. 2016;6:15345–15353. doi:10.1039/C5RA25214H
30. Guo B, Feng G, Manghnani PN, et al. The porphyrin-based conjugated polymer for highly efficient in vitro and in vivo photothermal therapy. *Small*. 2016;12:6243–6254. doi:10.1002/smll.201602293
31. Hamamura T, Dy JT, Tamaki K, et al. Dye-sensitized solar cells using ethynyl-linked porphyrin trimers. *Phys Chem Chem Phys*. 2014;16:4551–4560. doi:10.1039/c3cp55184a
32. Wang Y, Wang H, Liu D, Song S, Wang X, Zhang H. Graphene oxide covalently grafted upconversion nanoparticles for combined NIR mediated imaging and photothermal/photodynamic cancer therapy. *Biomater*. 2013;34:7715–7724. doi:10.1016/j.biomaterials.2013.06.045
33. Rossi LM, Silva PR, Vono LLR, Fernandes AU, Tada DB, Baptista MS. Protoporphyrin IX nanoparticle carrier: preparation, optical properties, and singlet oxygen generation. *Langmuir*. 2008;24:12534. doi:10.1021/la800840k
34. Tsolekile N, Nelana S, Oluwafemi OS. Porphyrin as diagnostic and therapeutic agent. *Molecules*. 2019;24:2669. doi:10.3390/molecules24142669
35. Radhakrishnan VS, Mukherjee S, Mukherjee S, Singh SP, Prasad T, Prasad T. ZnO quantum dots: broad spectrum microbicidal agent against multidrug-resistant pathogens E. coli and C. albicans. *Front Nanotechnol*. 2020;2:576342. doi:10.3389/fnano.2020.576342